The International Archives of the Photogrammetry, Remote Sensing and Spatial Information Sciences, Volume XLVIII-M-9-2025
30th CIPA Symposium "Heritage Conservation from Bits:
From Digital Documentation to Data-driven Heritage Conservation", 25–29 August 2025, Seoul, Republic of Korea

Digital Rubbing through Physical Simulation: A Non-Invasive Computational Approach for Epigraph Preservation

Hanyu Xiang[1, 2], Fan Zhang[1, 2, 3], Xueyi Wang[1, 2], Jiawei Liu[1, 2], Ao Tian[1, 2], Yiwen Zhu[4], Junping Gao[5], Xianfeng Huang[1, 2, 3, *]

[1] LIESMARS, Wuhan University, China - (xianghy, zhangfan, 2022286190129, 2024206190039, huangxf)@whu.edu.cn
[2] ICLCH, Wuhan University, China - (xianghy, zhangfan, 2022286190129, 2024206190039, huangxf)@whu.edu.cn
[3] Archaeological Institute for Yangtze Civilization, Wuhan University, China - (zhangfan, huangxf)@whu.edu.cn
[4] School of Geodesy and Geomatics, Wuhan University, China - 2022302141066@whu.edu.cn
[5] Longmen Grottoes Academy, China - junpinggao@126.com

Keywords: Inscription Relics, Epigraph Preservation, Digital Rubbing, Physical Simulation.

Abstract

The preservation of ancient Chinese inscription relics, including oracle bones, steles, and precious metal artifacts, faces critical challenges due to irreversible degradation from environmental erosion and physical contact during documentation. While traditional rubbing techniques remain widely used for recording surface inscription information, their mechanical ink-transfer process inherently causes cumulative damage through repetitive hammering and pressure application. This paper presents a novel computational framework through physical process simulation for non-invasive digital rubbing generation. Our key innovation lies in mathematically modeling the complex physical interactions involved in manual rubbing processes, including: (1) a *Xuan* paper generation model based on water retention properties, (2) a paper deformation model based on local depth, (3) an ink diffusion model based on contact probability. Experiments on ancient Chinese steles demonstrate our method's superior visual fidelity over existing digital methods, particularly in restoring ink textures resembling actual rubbings.

1. Introduction

Among ancient Chinese cultural relics, steles contain multiple cultural elements, including characters, decorative patterns, and sculptural carvings. They integrate history, literature, calligraphy, and sculpture, and possess significant historical, cultural, and artistic value. However, many stele inscriptions have become illegible due to natural weathering, biological erosion, and other factors. More severely, some steles have suffered substantial damage from natural disasters or human vandalism. For example, the Eastern Han dynasty's *Xiyue Huashan Temple Stele* was destroyed in an earthquake, the Three Kingdoms period's *Wu Tianxi Merit Stele* was burned in a fire, and the Tang dynasty's *Jiucheng Palace Sweet Spring Inscription* has been defaced with tourist graffiti like "visited here".

Rubbing, an ancient Chinese technique, involves using *Xuan* paper and ink to reproduce characters and patterns. The process entails placing moistened *Xuan* paper over uneven inscriptions, gently tapping it with a brush to conform to recessed areas, applying ink evenly when the paper is nearly dry, and finally peeling it off to produce a high-contrast rubbing. As rubbings are direct reproductions, their characters and patterns match the original in size and shape. Even if the original stele is later damaged, its content can be preserved through rubbing-based reproductions. For instance, the Tang dynasty's *Confucian Temple Stele* was destroyed shortly after erection but was later recarved based on rubbings, allowing this important artifact to survive in near-original form.

However, traditional manual rubbing requires direct contact with the stele surface, posing risks of damage. The process also demands strict environmental conditions, making it susceptible to weather, location, and other external factors. Additionally, results vary significantly depending on the operator's skill. These limitations hinder the application of traditional rubbing techniques to China's vast collection of ancient steles.

In recent years, 3D laser scanning has been widely adopted for digital preservation and rubbing generation of steles. The workflow involves capturing surface point clouds, processing data, and creating 3D models to extract depth information, which is then converted into grayscale rubbing images via digital image processing. While entirely contactless, such depth-based digital rubbings merely map surface relief directly, resulting in visual effects that differ markedly from traditional rubbings.

To address these issues, we propose a contactless digital rubbing method based on physical process simulation, systematically constructing a complete physical model of traditional rubbing production. First, we develop a *Xuan* paper model based on water retention properties to simulate absorption and ink diffusion. Second, we build a paper deformation model based on local depth to characterize the paper's conformity to the stele surface. Finally, we design an ink diffusion model based on contact probability to replicate authentic ink deposition patterns. Our method digitally simulates the entire "paper preparation-application-tapping-inking" workflow, avoiding physical contact damage while resolving the current digital rubbings' poor visual fidelity.

2. Related Work

2.1 Digital Rubbing Methods Based on Image Processing

Early research focused on binarization to convert images into black-and-white formats. For example, Wang *et al.* proposed combining 2D Otsu or triangle threshold segmentation with anisotropic diffusion for calligraphy documents to preserve character boundaries (Wang and Lee, 2001). Zhu *et al.* developed

* Corresponding author

a pipeline converting color stele photos into digital rubbings via enhancement and Otsu binarization to emulate traditional “recessed-white, raised-black” features (Zhu and Wu, 2008, Zhu et al., 2009, Zhu, 2010). Hu *et al.* generated orthophotos from laser point clouds, applying adaptive local thresholds with Otsu binarization to achieve measurable digital rubbings while simulating edge blurring (Hu et al., 2017).

Although simple, such binarization methods only suit images with clear foreground-background separation. Edge-based algorithms emerged for more precise inscription contour capture. Zhang *et al.* proposed a principal component analysis-based curvature scale space method to detect and approximate character contours as scalable parametric curves (Zhang et al., 2007). Lu *et al.* introduced local standard deviation mean ratio and unsharp operators to enhance edge detection of blurred details (Lu et al., 2010).

However, these approaches still struggled to replicate the distinctive ink textures of manual rubbings. To overcome this, researchers turned to simulation techniques. Zhong *et al.* modeled *Xuan* paper physics and ink solute diffusion equations to simulate penetration and spreading (Wu et al., 2014). Wu et al. created an ink texture library and used digital distance transforms to align textures with character boundaries (Wu et al., 2015). Both achieved realistic ink texture reproduction.

Image-based approaches require controlled photography conditions and high resolution, yet many aged steles have indistinct textures that are difficult to capture in 2D. This spurred the development of 3D model-based approaches.

2.2 Digital Rubbing Methods Based on 3D Models

These methods generate rubbing images from high-precision point clouds or mesh data.

Hui *et al.* manually constructed Delaunay triangulations to produce rubbings from depth maps, but the results were coarse and labor-intensive (Hui, 2015). Zhang *et al.* introduced plane fitting for depth map extraction, though large uneven steles produced saddle-shaped fits, causing uneven shading (Zhang, 2018). Pan *et al.* improved this via local depth calculations simulating rubbing pad radii, but ink texture simulation remained inadequate (Pan et al., 2019). Nie *et al.* employed 3D baking with displacement maps, surface curvature, and ambient occlusion for high-fidelity results, albeit with high computational costs (Nie, 2023).

In summary, existing digital rubbing methods suffer from low automation, sensitivity to stele quality, and insufficient realism. Authentic ink texture replication requires deeper integration of traditional techniques.

3. Manual Rubbing Process

As intangible cultural heritage, rubbing-making involves meticulous steps: (1) applying moistened *Xuan* paper to the stele, (2) tapping with a palm-fiber brush to reveal recesses and raises, (3) inking with even strokes using a rubbing pad when the paper is nearly dry (Su, 2022). Figure 1 illustrates the process (Wu and Zheng, 2022). This skill-demanding process yields variable results and has low efficiency, with preservation challenges necessitating improved production and display methods.

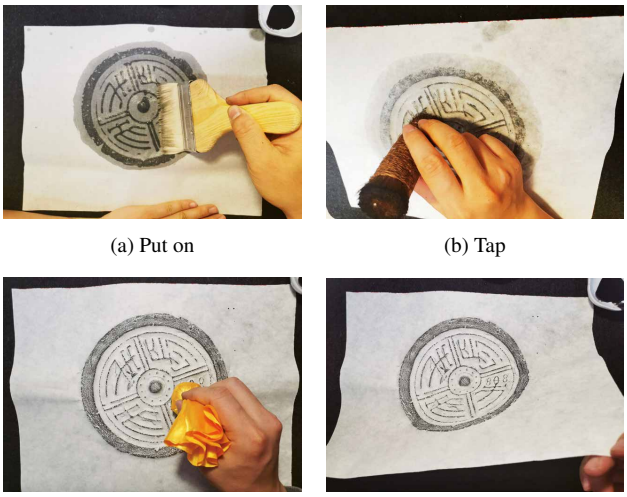

(a) Put on (b) Tap

(c) Ink (d) Peel off

Figure 1. Illustrations of the manual rubbing process.

4. Methods

Our approach systematically analyzes the physics of manual rubbing and employs computer simulation to generate high-fidelity digital rubbings.

4.1 Water Retention-Based Xuan Paper Model

During the rubbing-making process, ink textures primarily depend on two factors: (1) variations in carving depth on the stele surface, and (2) the water absorption properties of Xuan paper. Papers with different absorption characteristics yield distinct ink gradations and visual effects (Chu and Tai, 2005). Furthermore, finished rubbings retain the natural texture of *Xuan* paper, which has become an essential artistic feature of rubbing art. Thus, precisely analyzing and simulating *Xuan* paper’s physical structure and absorption properties are fundamental for emulating manual rubbing techniques.

Guo et al. provided a 500x microscopic view of paper fiber structure, where white areas represent fibers and black areas indicate voids as shown in Figure 2a (Guo and Kunii, 1991). Variations in fiber structure, paper density, and fiber distribution uniformity influence ink texture formation. This paper adopts the *Xuan* paper model proposed by Wang et al., which directly simulates the stochastic nature and diffusion capacity of Xuan paper with computational efficiency (Wang, 2008).

A “paper unit” is defined as the minimal divisible area of *Xuan* paper, typically set to one pixel. Experiments demonstrate that regions with higher paper density exhibit stronger diffusion capacity and greater ink storage. Thus, each unit’s fundamental attributes include saturated water retention capacity and spatial position. To simulate paper inhomogeneity, normally distributed random numbers are generated for saturation parameters for each unit using the following formula:

$$N(i,j) = N_0 + \sigma\sqrt{-2\ln r_1}\cos(2\pi r_2), \tag{1}$$

where $N(i,j)$ is the saturated water retention capacity at location (i,j), N_0 is the average water retention capacity of *Xuan* paper, σ is the maximum offset of water retention capacity, and r is a random number within the range of $[0,1]$.

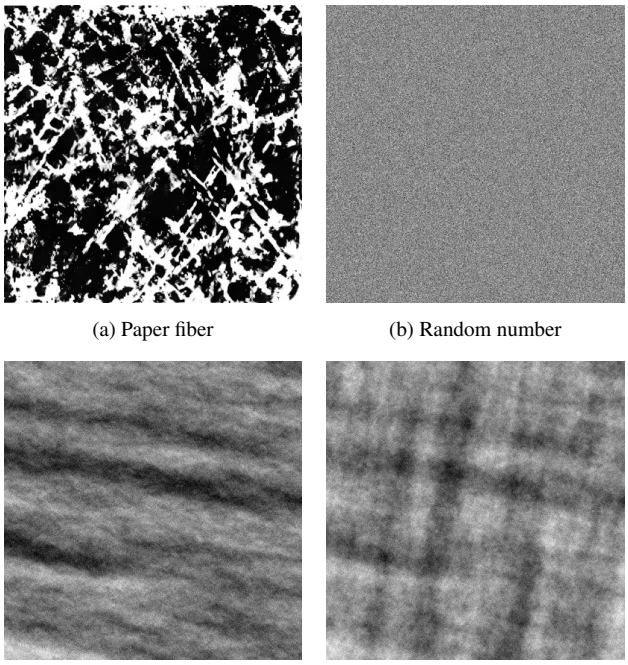

(a) Paper fiber (b) Random number

(c) L-neighborhood (d) L-neighborhood + Rotation

Figure 2. Illustrations of the *Xuan* paper model.

With average water retention $\mu = 200$ and offset $\sigma = 10$, the above formula generates *Xuan* paper as shown in Figure 2b. Brighter regions indicate stronger water retention and conductivity, while darker areas denote weaker capacity. Zero brightness signifies no absorption and conduction functionality.

To emulate *Xuan* paper's global uniform yet locally stochastic nature, local water retention continuity must be maintained. We calculate retention values using an L-neighborhood method, defining each unit's value as the mean of its preceding synthesized neighbors:

$$N(i,j) = \frac{1}{n}\sum N(x,y) + \sigma\sqrt{-2\ln r_1}\cos(2\pi r_2), \quad (2)$$

where $N(x,y)$ is the L-neighborhood pixel , and n is the number of pixels in the L-neighborhood.

With average water retention $\mu = 200$, offset $\sigma = 10$, and neighborhood radius $r = 2$, the formula produces paper shown in Figure 2c. We rotate and overlay these simulated patterns to create combined textures that resemble actual *Xuan* paper (Figure 2d).

4.2 Local Depth-Based Paper Deformation Model

During the rubbing process, moistened *Xuan* paper is carefully applied to the engraved stele surface and repeatedly tapped with a palm-fiber brush until the paper fully conforms to the surface contours, revealing clear impressions of inscriptions and patterns. Building upon traditional hammering techniques used in manual rubbing, we develop a mathematical deformation model to digitally simulate paper conformation after hammering.

Using 3D laser scanning technology, we perform non-invasive digitization of steles to generate precise polygonal mesh models represented as $M = \{V, E\}$, where V is the set of vertices and E is the set of edges.

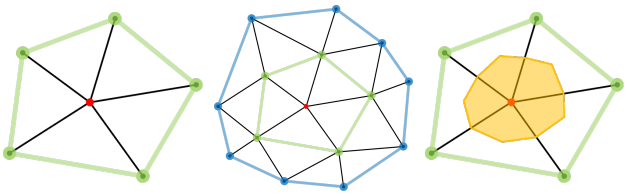

(a) 1-ring (b) 2-ring (c) Barycentric cell

Figure 3. Illustrations of geometric search and vertex weight.

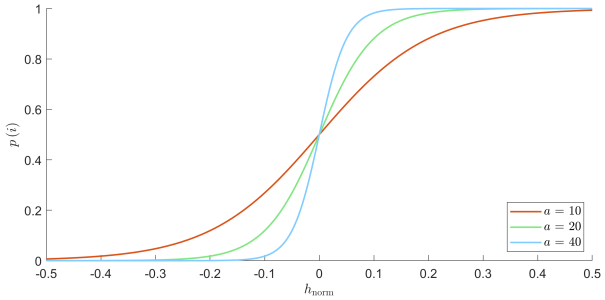

Figure 4. The *Sigmoid* function with different *a* coefficients.

To simulate the physical dimensions of rubbing tools, we first compute the average edge length $\bar{l}$ of the mesh and define the maximum effective distance of the rubbing pad as $d_{\max} = k \times \bar{l}$. For each vertex $v_i \in V$, we construct its neighborhood $N(v_i)$ through geometric search. We define the n-ring neighborhood of v_i as the set of reachable vertices within path length n (Figures 3a and 3b). The generation process of $N(v_i)$ starts from the 1-ring neighborhood and expands outward, ring by ring, until all new n-ring vertices exceed $d_{\max}$ in geodesic distance from v_i. Then, a weighted least-squares plane P_i is fitted to $N(v_i)$, with weights w_j proportional to the barycentric cell area of each $v_j \in N(v_i)$ (Figure 3c). Larger cells indicate more obvious planar features and receive higher weights to emphasize their geometric influence. Finally, the local depth d_i of v_i is computed as its signed distance to P_i.

Based on the local depth information, we establish a probability model for the contact between the rubbing pad and the stele surface. Using depth statistics (mean μ_h and standard deviation σ_h), three zones are defined:

$$p(i) = \begin{cases} 1 \text{ (Raise zone)} & h_i \geq \mu_h + 3\sigma_h \\ 0 \text{ (Recess zone)} & h_i \leq \mu_h - 3\sigma_h \\ \dfrac{\exp\left(a\tilde{h}_i\right)}{1+\exp\left(a\tilde{h}_i\right)} \text{ (Transition zone)} & \text{else,} \end{cases}$$

where $\tilde{h}_i = \dfrac{h_i - \mu_h}{6\sigma_h}$ is the normalized depth. We adopt the *Sigmoid* function for the transition zone to achieve a smooth probability mapping from 0 to 1, reflecting the possibility of contact between the rubbing pad and the surface at different depths (Figure 4).

4.3 Contact Probability-Based Ink Diffusion Model

Xuan paper exhibits excellent liquid absorption and permeability, enabling ink diffusion across its surface. This diffusion process is primarily driven by ink concentration gradients.

According to Fick's law of diffusion, the mass transfer dm through a unit area dS along normal direction $\vec{n}$ during a time

interval dt is given by:

$$dm = -D\frac{\partial \rho}{\partial n}dSdt, \tag{3}$$

where D is the diffusion coefficient, and the negative sign indicates flow from high to low concentration. For any closed region Ω with boundary $\partial\Omega$, the inflow mass during $[t_1, t_2]$ is:

$$\begin{aligned} m_1 &= \int_{t_1}^{t_2} \left\{ \iint_{\partial\Omega} D\frac{\partial \rho}{\partial n}dS \right\} dt, \\ m_1 &= \int_{t_1}^{t_2} \left\{ \iiint_{\Omega} \left\{ \frac{\partial}{\partial x}\left(D\frac{\partial \rho}{\partial x}\right) + \frac{\partial}{\partial y}\left(D\frac{\partial \rho}{\partial y}\right) \right.\right. \\ &\quad \left.\left. + \frac{\partial}{\partial z}\left(D\frac{\partial \rho}{\partial z}\right) \right\} dV \right\} dt. \end{aligned} \tag{4}$$

Meanwhile, the temporal concentration change $\Delta\rho$ corresponds to mass variation:

$$\begin{aligned} m_2 &= \iiint_{\Omega} \Delta\rho dV = \iiint_{\Omega} \left(\int_{t_1}^{t_2} \frac{\partial \rho}{\partial t}dt \right) dV \\ &= \int_{t_1}^{t_2} \left(\iiint_{\Omega} \frac{\partial \rho}{\partial t}dV \right) dt \end{aligned} \tag{5}$$

The mass conservation principle equates spatial and temporal changes, giving $m_1 = m_2$:

$$\frac{\partial \rho}{\partial t} = \frac{\partial}{\partial x}\left(D\frac{\partial \rho}{\partial x}\right) + \frac{\partial}{\partial y}\left(D\frac{\partial \rho}{\partial y}\right) + \frac{\partial}{\partial z}\left(D\frac{\partial \rho}{\partial z}\right). \tag{6}$$

Simplified to 2D plane, the diffusion equation becomes:

$$\frac{\partial \rho}{\partial t} = \frac{\partial}{\partial x}\left(D\frac{\partial \rho}{\partial x}\right) + \frac{\partial}{\partial y}\left(D\frac{\partial \rho}{\partial y}\right). \tag{7}$$

Ink diffusion occurs primarily within *Xuan* paper's internal structure, governed by its fiber spatial distribution. When a paper unit reaches saturation, its water conductivity peaks but decreases with drying. Thus, the water diffusion coefficient follows:

$$D(\rho) = D_0 \exp\left(-\beta\left(\rho_0 - \rho\right)\right), \tag{8}$$

where D_0 is the saturated water conductivity, and β is the empirical constant.

Ink solute transport includes ink convection driven by water diffusion and ink diffusion caused by ink solute concentration gradients. Experimental studies show that the ink convection caused by water movement always dominates, while the ink solute diffusion can be neglected in comparison (Wang, 2008).

Based on the above ink diffusion model, we analyze the traditional manual rubbing process: (1) **Paper Application Stage:** Evenly apply clean water with a brush, when the *Xuan* paper is almost dry but slightly damp, paper units obtain initial water concentration ρ^0_{water}. (2) **Inking Stage:** Evenly apply ink through the rubbing pad and lightly tap the stele, achieving layered ink darkening through multiple repetitions.

Our model replicates traditional rubbing through iterative steps. Paper units have initial water content:

$$m^0_{\text{water}}(i,j) = N(i,j) \times \rho^0_{\text{water}}, \tag{9}$$

where $N(i,j)$ is the saturated water retention capacity at location (i,j). Each inking has fixed ink content (water content Δm_{water} and ink concentration ρ_{ink}). According to the contact probability model (Section 4.2), the actual water and ink content obtained by paper units is:

$$\begin{aligned} \Delta m_{\text{water}}(i,j) &= p(i,j) \times \Delta m_{\text{water}}, \\ \Delta m_{\text{ink}}(i,j) &= \rho_{\text{ink}} \times \Delta m_{\text{water}(i,j)}. \end{aligned} \tag{10}$$

Then, update water and ink concentration:

$$\begin{aligned} \rho^{n+1}_{\text{water}}(i,j) &= \frac{m^n_{\text{water}}(i,j) + \Delta m_{\text{water}}(i,j)}{N(i,j)}, \\ \rho^{n+1}_{\text{ink}}(i,j) &= \frac{m^n_{\text{ink}}(i,j) + \Delta m_{\text{ink}}(i,j)}{m^n_{\text{water}}(i,j) + \Delta m_{\text{water}}(i,j)}. \end{aligned} \tag{11}$$

Finally, calculate ink diffusion based on Equations 7 and 8.

Through multiple iterations of this process, we successfully replicate the ink texture characteristics of manual rubbings. Notably, the ink content no longer increases after the inking stage, but the diffusion process continues. Therefore, subsequent iterations simulate only natural permeation until stabilization without adding new ink content.

5. Experiments

In our experiments, we select the Ming dynasty's *Shanhua Stele* for testing. The generated *Xuan* paper has an average water retention capacity of 200, offset of 10, and *L*-neighborhood radius of 2. The maximum effective distance coefficient of the rubbing pad is 10. The probability mapping coefficient of the *Sigmoid* function is 40. The saturated water conductivity of paper units is 0.2, with an empirical constant of 0.02. The number of inking iterations is 50. For comparison, we use manual rubbings as reference and select non-photorealistic rendering (Wegen et al., 2024, Ribes and Boucheny, 2011) and local-depth mapping (Pan et al., 2019) as comparative methods.

Figures 5 and 6 illustrate the rendered images with and without textures, and the manual rubbings of *Shanhua Stele*. The inscriptions are hard to recognize in the rendered images, but clear in the manual rubbings.

Figures 7 and 8 show digital rubbing results at different scales. Experiments show our method outperforms existing digital methods in visual fidelity, particularly in restoring authentic ink textures, with results more closely resembling real rubbings.

The importance of diffusion coefficient D_0 in the ink diffusion process is shown in Figure 9. When D_0 takes smaller values, water penetration is weaker, resulting in smaller seepage flows and less noticeable convection of ink solutes following water movement; the opposite occurs with larger values. Results from different numbers of inking iterations are shown in Figure 10. As iteration count increases, ink darkness progressively deepens.

6. Conclusion

This study presents a novel computational framework for generating digital rubbings through physics-based simulation, addressing critical challenges in the non-invasive preservation of ancient Chinese inscription relics. Our method systematically

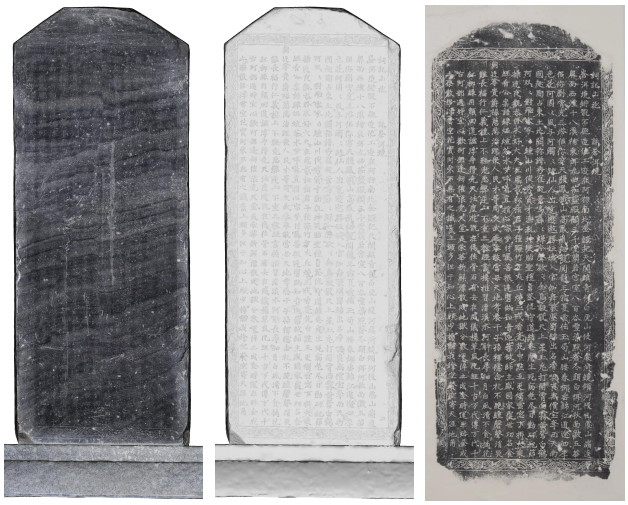

(a) Rendered image with texture (b) Rendered image without texture (c) Manual rubbing

Figure 5. Illustrations of the orthogonal projections and the manual rubbing of *Shanhua Stele - Southern side*.

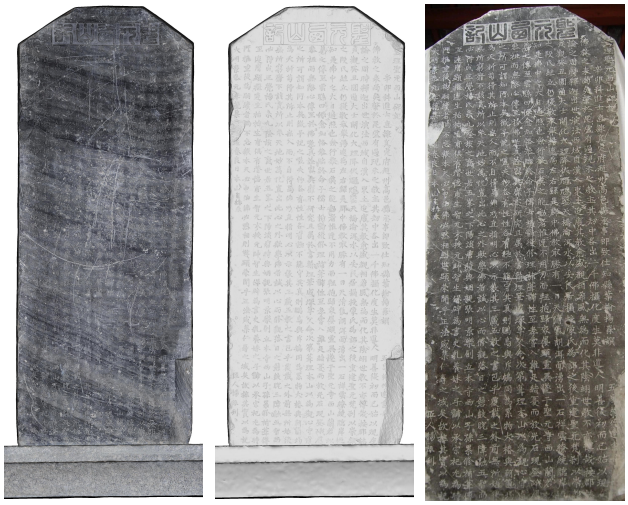

(a) Rendered image with texture (b) Rendered image without texture (c) Manual rubbing

Figure 6. Illustrations of the orthogonal projections and the manual rubbing of *Shanhua Stele - Northern side*.

models three key physical processes: (1) *Xuan* paper generation via water retention properties, (2) paper deformation based on local depth analysis, and (3) ink diffusion dynamics through contact probability mapping. Experimental results on the Ming dynasty's *Shanhua Stele* demonstrate superior visual fidelity compared to existing digital methods, particularly in reproducing authentic ink textures and preserving subtle epigraphic details. The main limitation arises when processing severely damaged surfaces, where local depth estimation becomes unreliable due to missing or fragmented surface features. Future work will integrate non-photorealistic rendering techniques to better capture surface relief, combined with our ink diffusion model to achieve more authentic digital rubbing effects.

7. Acknowledgments

This work was supported by Tanyuan Plan 2024.

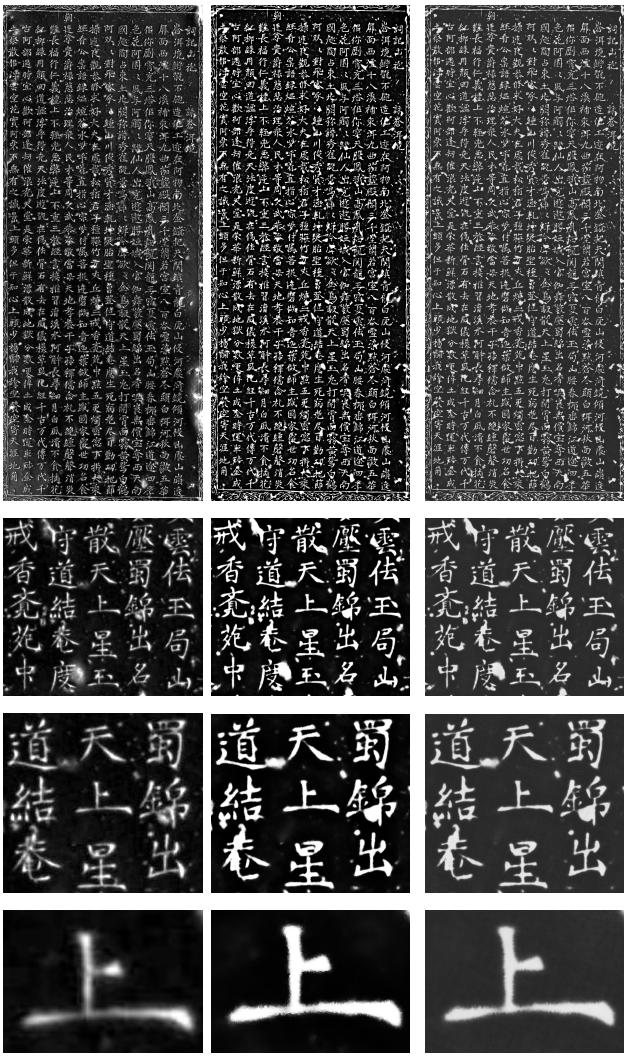

(a) Non-photorealistic rendering (b) Local-depth mapping (c) Ours

Figure 7. Illustrations of the digital rubbing results of *Shanhua Stele - Southern side* at different scales.

References

Chu, N. S.-H., Tai, C.-L., 2005. Moxi: Real-Time Ink Dispersion in Absorbent Paper. *ACM Transactions on Graphics (TOG)*, 24(3), 504–511.

Guo, Q., Kunii, T. L., 1991. Modeling the diffuse paintings of ‘sumie’. *Modeling in Computer Graphics*, 329–338.

Hu, C., Xue, H., Xia, G., Zhang, X., Hou, Y., 2017. Digital Rubbings Generating Method Based on Laser Point Clouds and Close-Range Images. *Laser Journal*, 38(9), 32–37.

Hui, P., 2015. Method for Extracting Stele Inscription Digital Rubbing Based on Three-Dimensional Data Scanning.

Lu, X., Taiyi, Z., Zhang, Y., Junling, D., 2010. A New Edge Detecting Algorithm Based on Local Characteristic in Rubbings’ Processing. *Microelectronics & Computer*, 97–100.

Nie, F., 2023. Digital Rubbing Generation and Virtual Display of Epitaphs. *Popular Archaeology*, 48–53.

Pan, R., Tang, Z., Da, W., 2019. Digital Stone Rubbing from 3D Models. *Journal of Cultural Heritage*, 37, 192–198.

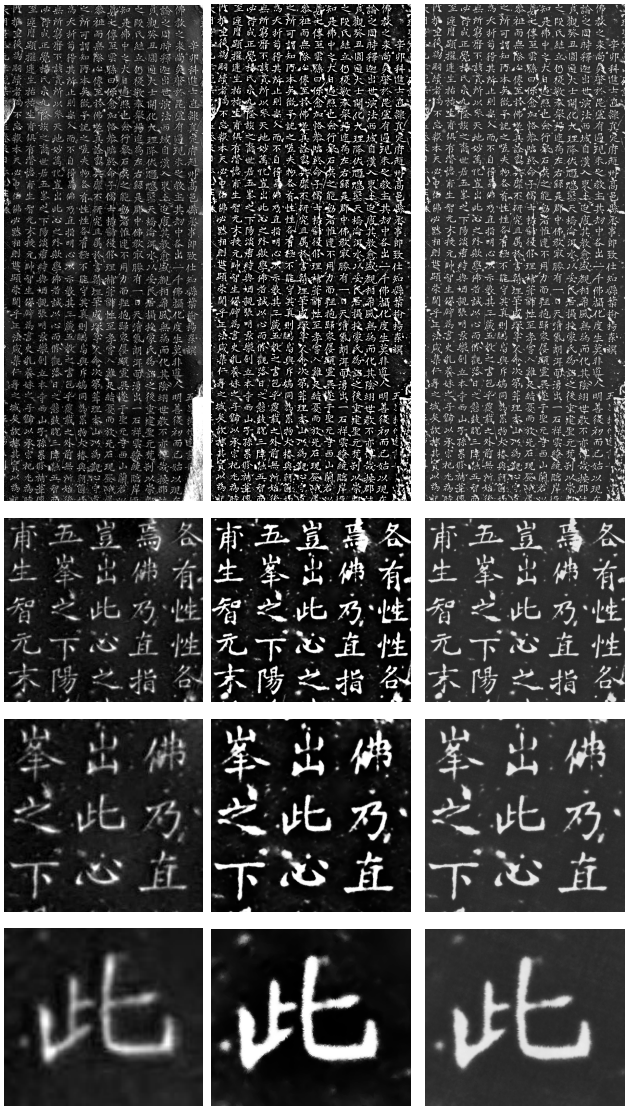

(a) Non-photorealistic rendering (b) Local-depth mapping (c) Ours

Figure 8. Illustrations of the digital rubbing results of *Shanhua Stele - Northern side* at different scales.

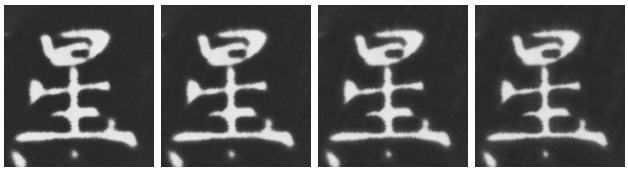

(a) $D_0 = 0.1$ (b) $D_0 = 0.2$ (c) $D_0 = 0.4$ (d) $D_0 = 0.8$

Figure 9. The importance of diffusion coefficient D_0 in the ink diffusion process.

Ribes, A., Boucheny, C., 2011. Eye-Dome Lighting: A Non-Photorealistic Shading Technique. *Kitware Source Quarterly Magazine*, 7.

Su, H., 2022. Research on the Generation Process and Techniques of Historical and Cultural Rubbings. *Yellow River Yellow Earth Yellow Race*, 59–61.

Wang, S.-Z., Lee, H.-J., 2001. Dual-binarization and anisotropic diffusion of chinese characters in calligraphy documents.

(a) Iter. = 10 (b) Iter. = 30 (c) Iter. = 50

Figure 10. Results from different numbers of inking iterations.

Proceedings of Sixth International Conference on Document Analysis and Recognition, 271–275.

Wang, X., 2008. Research on the Simulation of Chinese Painting. PhD thesis, Tianjin University.

Wegen, O., Scheibel, W., Trapp, M., Richter, R., Dollner, J., 2024. A Survey on Non-Photorealistic Rendering Approaches for Point Cloud Visualization. *IEEE Transactions on Visualization and Computer Graphics*, 1-20.

Wu, J., Zheng, Z., 2022. Manual Rubbing Generation of ”Changle Weiyang” tiles. *Calligraphy Education*, 79–85.

Wu, X., Zhong, H., Wen, P., 2014. Digital rubbings creation based on ink diffusion. *2014 IEEE International Conference on Information and Automation (ICIA)*, 914–919.

Wu, X., Zhong, H., Wen, P., 2015. Texture mapping based digital rubbing method. *2015 IEEE International Conference on Mechatronics and Automation (ICMA)*, 2363–2368.

Zhang, J., Yu, J., Lin, H., 2007. Capturing character contours from images of ancient chinese calligraphy. *Second Workshop on Digital Media and its Application in Museum & Heritages*, 36–41.

Zhang, Y., 2018. The Generation and Application of Digital Rubbing of Inscriptions Based on 3D Model. PhD thesis, Zhejiang University.

Zhu, X., 2010. A Schematic Analysis of Stone Inscriptions of Song Tombs in South Sichuan and Research of Digital Rubbings. PhD thesis, Chongqing University.

Zhu, X., Wu, Z., 2008. Technical Study on Photoshop Based Relief Image Digital Rubbings. *Computer Science*, 35(12), 224–228.

Zhu, X., Wu, Z., Li, Y., 2009. Study on MATLAB Based Stone Relief Image Digital Rubbing Technique. *Computer Science*, 36(2), 268–270.